APPLIED OPTICS

Laser soliton microcombs heterogeneously integrated on silicon

Chao Xiang[1]†, Junqiu Liu[2]†, Joel Guo[1], Lin Chang[1], Rui Ning Wang[2], Wenle Weng[2], Jonathan Peters[1], Weiqiang Xie[1], Zeyu Zhang[1], Johann Riemensberger[2], Jennifer Selvidge[3], Tobias J. Kippenberg[2]*, John E. Bowers[13]*

Silicon photonics enables wafer-scale integration of optical functionalities on chip. Silicon-based laser frequency combs can provide integrated sources of mutually coherent laser lines for terabit-per-second transceivers, parallel coherent light detection and ranging, or photonics-assisted signal processing. We report heterogeneously integrated laser soliton microcombs combining both indium phosphide/silicon (InP/Si) semiconductor lasers and ultralow-loss silicon nitride (Si_3N_4) microresonators on a monolithic silicon substrate. Thousands of devices can be produced from a single wafer by using complementary metal-oxide-semiconductor–compatible techniques. With on-chip electrical control of the laser-microresonator relative optical phase, these devices can output single-soliton microcombs with a 100-gigahertz repetition rate. Furthermore, we observe laser frequency noise reduction due to self-injection locking of the InP/Si laser to the Si_3N_4 microresonator. Our approach provides a route for large-volume, low-cost manufacturing of narrow-linewidth, chip-based frequency combs for next-generation high-capacity transceivers, data centers, space and mobile platforms.

Optical frequency combs (OFCs) (*1*, *2*) have revolutionized timing, spectroscopy and metrology. Discovered a decade ago, OFCs can be generated in optical microresonators where bright dissipative Kerr solitons are formed (*3*). These types of OFCs are referred to as "soliton microcombs" and have already been used in system-level applications. In parallel, there has been substantial progress in photonic integrated platforms for microcomb generation, among which Si_3N_4 (*4*–*7*, *8*, *9*) has emerged as the most mature and widely used platform. Recent advances in fabrication of nonlinear, dispersion-engineered, Si_3N_4 photonic integrated circuits (PICs) have enabled optical losses below 1 dB/m (*8*, *9*), resulting in soliton formation with milliwatt threshold power levels that integrated lasers can provide and repetition rates in the microwave X-band (*10*). Combining with negligible thermal effects and Kerr-dominated frequency-dependent response (*9*), reliable soliton generation can be attained without complex or fast laser tuning. Additionally, laser self-injection locking (*11*–*14*) and hybrid integration of soliton microcombs with distributed feedback (DFB) lasers (*15*–*17*) and reflective semiconductor optical amplifiers (RSOAs) (*18*) allow for current-initiated and electrically controlled modules with low electrical power.

[1]Department of Electrical and Computer Engineering, University of California, Santa Barbara, Santa Barbara, CA 93106, USA. [2]Institute of Physics, Swiss Federal Institute of Technology Lausanne (EPFL), CH-1015 Lausanne, Switzerland. [3]Materials Department, University of California, Santa Barbara, Santa Barbara, CA 93106, USA.
*Corresponding author. Email: tobias.kippenberg@epfl.ch (T.J.K.); bowers@ece.ucsb.edu (J.E.B.)
†These authors contributed equally to this work.

A long-standing goal is to monolithically integrate lasers and high-Q nonlinear microresonators onto a common silicon wafer. Heterogeneously integrated silicon photonics (*19*–*21*) offers a compelling solution using low-cost, industry-standard silicon substrates, aided by mature complementary metal-oxide-semiconductor (CMOS)–compatible fabrication facilities. High-performance, large-scale heterogeneous PICs with complete functionalities are disrupting optical interconnect technology and other applications (*22*, *23*). However, heterogeneous integration of high-power, narrow-linewidth semiconductor lasers with high-Q Si_3N_4 microresonators has not been demonstrated yet, because multiple material platforms (Si, Si_3N_4, and III-V) with appreciably different optical properties have to be deployed and combined. Here we overcome these challenges and present the first demonstration of heterogeneously integrated laser soliton microcombs. A chip-scale laser frequency comb (Fig. 1A, top) consists of three main parts: a DFB laser, a thermo-optic phase tuner, and a high-Q nonlinear microresonator, combined by leveraging multilayer heterogeneous integration (*24*). Here, the DFB laser, phase tuner, and nonlinear microresonator are built on InP/Si, Si, and Si_3N_4 layers, respectively (Fig. 1A, bottom inset). This vertical, multilayer structure is realized through sequential wafer bonding of a silicon-on-insulator (SOI) wafer and an InP multiple-quantum-well (InP MQW) epi wafer to a prepatterned Si_3N_4 substrate fabricated using the photonic Damascene process (*9*, *24*). Here we directly apply the heterogeneous integration on a 100-mm-diameter Si substrate and process the entire substrate on the wafer scale.

The continuous-wave laser output passes through a thermo-optic resistive heater (for optical phase control) and couples into a high-Q Si_3N_4 microring resonator where Kerr nonlinear four-wave mixing generates soliton microcombs. The Si_3N_4 microresonator exhibits anomalous group velocity dispersion (GVD) in the telecommunication C band and has a free spectral range (FSR) of 100 GHz. The laser directly pumps the microresonator without an intermediate optical isolator, and the entire device is electronically operated via laser current control and phase control. Laser self-injection locking (*11*, *12*, *13*, *14*) leverages the narrow-band optical feedback at desired phase relations from a high-Q microresonator to stabilize the pump laser and pulls the laser frequency toward the microring resonance. In this scenario, soliton microcombs can form when optimum laser-microresonator frequency detuning is reached. The DFB laser wavelength increases with increasing laser current, as the grating index increases as a result of injected electrical power heating. Consequently, certain gain currents trigger comb generation when the laser wavelength coincides with a microresonator resonance. The comb generation region resides where the laser is red-detuned to the resonance (Fig. 1B), and the phase of the Rayleigh backscattered light from the microresonator to the laser fulfills certain phase relations (*25*). Figure 1C shows photographs of the fabricated devices with difference scales.

Our fabrication process flow (Fig. 2A) starts with the photonic Damascene process (*7*, *9*) to fabricate the Si_3N_4 PIC on a Si substrate with 4-μm-thick thermal wet silicon dioxide (SiO_2). The PIC pattern is exposed with deep ultraviolet (DUV) stepper lithography and dry-etched into the SiO_2 substrate to form the waveguide preform. Stoichiometric Si_3N_4 is deposited on the patterned SiO_2 preform by using low-pressure chemical vapor deposition (LPCVD), filling the trenches and forming waveguide cores. Chemical-mechanical polishing (CMP) is used to remove excess Si_3N_4, planarize the wafer front surface, and control the Si_3N_4 waveguide height (780 nm). Afterward, spacer SiO_2 of 300-nm thickness is deposited on the Si_3N_4 substrate. The entire substrate is further annealed at 1200°C to drive out the residual hydrogen content in Si_3N_4 and SiO_2 and to densify the spacer SiO_2. A second CMP is performed to create a flat and smooth wafer surface. The measured root mean square (RMS) roughness of the wafer surface measured by atomic force microscopy (AFM) is 0.27 nm (Fig. 2B left), enabling direct substrate bonding with an SOI wafer.

To achieve high bonding yield, vertical channels for outgassing are etched before wafer bonding (*25*, *26*). Coarse alignment is required to bond blank films on the target areas of the

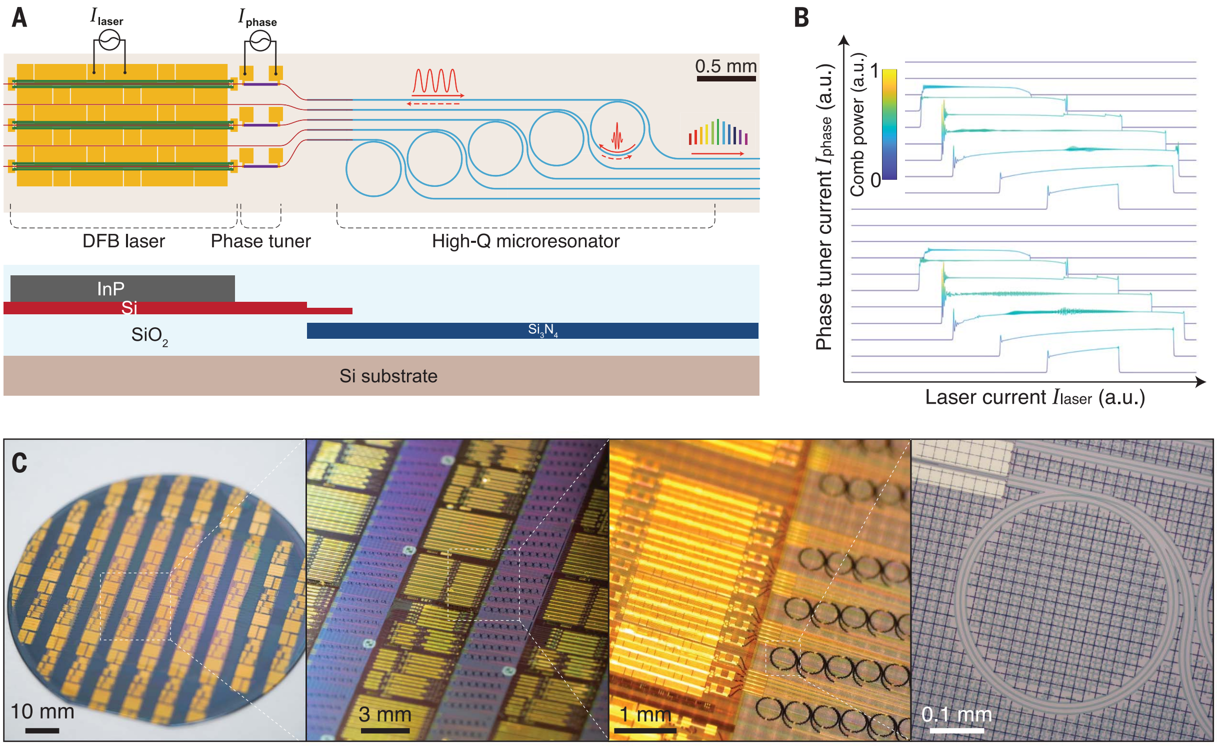

Fig. 1. Device schematic, images, and operation principle. (**A**) Schematic of laser soliton microcomb devices consisting of DFB lasers, phase tuners, and high-Q microresonators on a common substrate. A continuous-wave signal (solid red line) emitted from the laser is coupled into the microresonator and partially backscattered. The backscattered signal (dashed red line) to the laser triggers self-injection locking that assists soliton formation inside the microresonator. The locking is optimized by controlling the laser current I_{laser} and phase tuner current I_{phase}. The bottom inset shows the simplified device cross section. The laser is based on InP/Si, and the microresonator is based on Si_3N_4. The intermediate Si layer with two etch steps is used to deliver light from the InP/Si layer to the Si_3N_4 layer. (**B**) Schematic of the microcomb generation with sweeping laser current I_{laser} and varying phase tuner current I_{phase}, to control the optical phase of self-injection locking. This waterfall plot is based on a full nonlinear simulation (*25*). (**C**) Photographs showing the completed 100-mm-diameter wafer and zoom-in of multiple dies, and a microscopic image showing a Si_3N_4 microring resonator with Si/Si_3N_4 interface.

patterned substrate. Fine alignment of patterns on different layers with an accuracy within 100 nm is enabled by DUV stepper lithography. After removing the Si substrate and buried SiO_2 layer of the bonded SOI wafer, the Si device layer is processed to create waveguide structures with different etch depths, including shallow-etched Si rib waveguides for the lasers and phase tuners, fully etched hole structures for gratings (Fig. 2B, right), and thin Si tapers for mode conversion between the Si waveguide and underlying Si_3N_4 waveguide (*24*). InP-based MQW gain material is then bonded to the patterned Si device at the active regions. The InP process starts with InP substrate removal. InP mesa etches, including P-type InP, InAlGaAs MQW, and N-type InP, are performed by selective dry etching and wet etching. P- and N-type contact metals are deposited on the P-InGaAs layer and N-InP layer, respectively. The excess Si on top of Si_3N_4 microresonators is removed before laser passivation by hydrogen-free deuterated SiO_2 deposition (*27*). Vias are then etched for laser electrical contact, followed by proton implantation on the laser mesa structure to reduce electrical current leakage. Heater and probe metals are deposited at the end of the full process. Finally, the entire wafer is diced into dozens of dies or chips to facilitate testing. The InP/Si-to-Si rib waveguide transition loss is below 1 dB (*28*), and the Si-to-Si_3N_4 mode conversion efficiency is simulated to be above 90% (*25*). Assuming all devices share the same design, the overall device yield is determined primarily by the SOI bonding and InP bonding yields. In the current wafer, we have achieved bonding yields that enable thousands of complete laser-microresonator devices, each of which has a footprint as small as 1.6 mm^2 (*25*). Figure 2C shows the scanning electron microscopic (SEM) images of the device cross section, which is false-colored to illustrate the multilayer structure.

The experimental setup to characterize the final chip devices is shown in Fig. 3A. We first characterize the laser performance. The DFB laser is a high-power, single-longitudinal-mode pump source with a high side-mode suppression ratio (SMSR) such that the laser wavelength can be tuned to a microring resonance (*29*). Our laser has a 1.8-mm-long InP/Si gain section, and the grating is etched on both sides of the shallow-etched Si rib waveguide with a 170-nm gap separation from the Si waveguide core. The fully etched grating provides the optical resonant feedback for the pump laser and determines the lasing wavelength λ_{pump} by its pitch Λ ($\lambda_{pump} = 2n_{eff}\Lambda$). Here, $\Lambda = 238$ nm, n_{eff} ~3.26, and λ_{pump} ~1550 nm. A quarter-wavelength shift section is included at the grating length center to supply nondegenerate phase conditions favoring single-longitudinal-mode lasing. Figure 3B shows the measured light-current curves (solid blue), i.e., the laser output power versus stepped laser injection current, with 7-mA phase tuner current and 20°C stage temperature. The measured laser threshold current is 64 mA. The laser power is outcoupled from the Si_3N_4 waveguide inverse-taper to a lensed fiber. The maximum power in the output fiber is measured as 8 mW, and the corresponding on-chip power in the Si_3N_4 waveguide is ~20 mW. The center wavelength of the laser measured with a

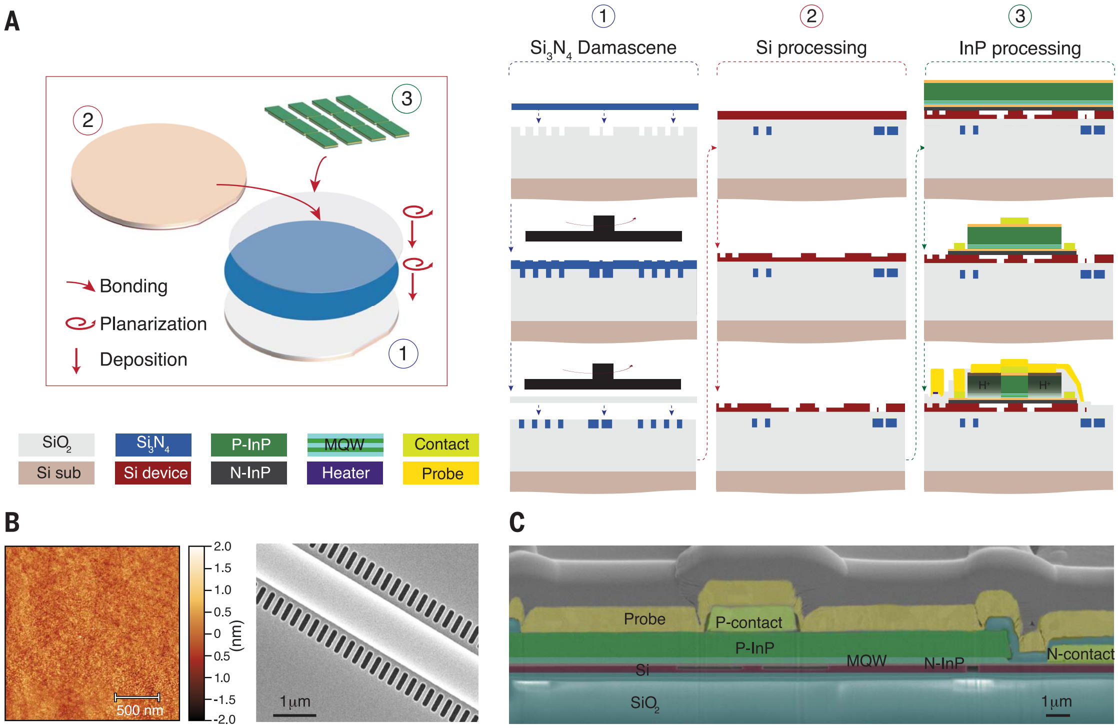

Fig. 2. Simplified wafer-scale fabrication process flow. (**A**) Multilayer heterogeneous integration process. Left panel shows that a prepatterned Si_3N_4 Damascene substrate is planarized and subsequently bonded with an SOI wafer and InP MQW epi pieces. Right panel shows selected key fabrication steps: (1) Si_3N_4 photonic Damascene process, including LPCVD Si_3N_4 deposition on the patterned SiO_2 substrate (top), excess Si_3N_4 removal and planarization via CMP (middle), and SiO_2 spacer deposition and polishing (bottom); (2) Si processing, including Si substrate removal (top), Si waveguide etch for laser and thermal tuner (middle) and for Si grating and Si-Si_3N_4 mode conversion taper (bottom); (3) InP processing, including InP substrate removal (top); InP mesa etch (middle); and excess Si removal, laser passivation, contact formation, vias open, heaters, and probe metal formation (bottom). All the photolithography steps are performed with a 248-nm DUV stepper, except that electron-beam lithography is used for the Si grating writing because of the required finer pattern resolution. Elements are not shown with the same scale so as to highlight the structures instead of the dimensions. (**B**) Left: Atomic force microscopy shows 0.27-nm RMS roughness of the Si_3N_4 wafer surface, after the second CMP on the SiO_2 spacer, before SOI bonding. Right: SEM image of Si grating for laser before InP bonding. (**C**) False-colored SEM image showing the cross section of the complete device in the laser area with multilayer structure.

wavelength meter is shown in Fig. 3B (dashed gray). Several dips on the light-current curve are observed at laser currents of 133.0, 231.0, 329.5, and 418.0 mA, where the laser wavelength coincides with microresonator resonances. These dips also verify the microresonator FSR of 100 GHz. A high-reflection coating is applied on the other side of the DFB laser to boost the laser output power. Future devices can avoid using this coating to yield mode-hop-free DFB lasers and linearized laser wavelength dependence on the laser current. The DFB laser has high SMSR at resonances #1 and #2, where high output powers are also obtained that are advantageous for comb generation. Figure 3C shows the single-longitudinal-mode laser spectra at two resonance wavelengths, with 60 and 57 dB SMSR, respectively.

Soliton microcomb is generated by aligning the laser frequency to the microresonator resonance via tuning the laser current, together with tuning the phase tuner current to control the relative forward to backward phase. As an optical isolator is absent between the laser and the Si_3N_4 microresonator, laser self-injection locking (*15*–*17*) occurs when the laser frequency coincides with a microresonator resonance. More information (*25*) about the phase dependence on comb generation is revealed by simulating the nonlinear self-injection locking process (*16*). In the critical coupling regime, the estimated Kerr parametric oscillation threshold is

$$P_{\mathrm{th}} = \frac{\pi n_0 \omega_{\mathrm{p}} A_{\mathrm{eff}}}{n_2 D_1 Q_0^2} \qquad (1)$$

where $\omega_p/2\pi \approx 193$ THz is the optical frequency of the pump mode, $n_0 = 2.0$ is the refractive index of Si_3N_4, $n_2 = 2.4 \times 10^{-19}\,\mathrm{m^2/W}$ is the nonlinear index of Si_3N_4, $A_{\mathrm{eff}} \approx 1.6 \times 10^{-12}\mathrm{m^2}$ is the effective mode area, $D_1/2\pi$ is the microresonator FSR, and Q_0 is the microresonator intrinsic quality factor. For Si_3N_4 microresonators of $Q_0 \sim 7 \times 10^6$ (*25*) and 100-GHz FSR used in this work, we estimate $P_{\mathrm{th}} \approx 2$ mW.

With a laser current around 329 mA, the estimated on-chip laser power required to pump the Si_3N_4 microresonator exceeds 16 mW. Perfect soliton crystal states (*30*) are observed by fine-tuning the laser frequency and the optical phase between the forward laser output and backward reflected signal (Fig. 3D). The access to soliton crystal states indicates that the pump laser power just reaches the soliton formation threshold (*25*). We also observe soliton crystal states with decreasing crystallization orders when increasing the laser current (red detuning). Further increasing the laser gain current to ~418 mA generates a two-soliton crystal state with 200-GHz line spacing and a single-soliton state with 100-GHz repetition rate. The coherent soliton nature is revealed by photodetection of the low-intensity noise from the comb lines beating. Once generated, the soliton states can be stable for hours in standard laboratory environments without any external feedback control. This stability benefits from the monolithic nature of the chip device and the laser-microresonator coupling through laser self-injection locking.

To further characterize the laser self-injection locking, we measure the frequency noise spectra of the pump line and comb lines in the single-soliton state and laser free-running state (Fig. 4A). Leveraging a high-*Q* external cavity, self-injection locking exhibits frequency noise reduction, i.e., laser linewidth narrowing (*13*). The fundamental linewidth of the free-running DFB laser is ~60 kHz and is reduced to ~25 Hz in the self-injection–locked single soliton state. Noise reduction of 10 dB is observed at 1-kHz Fourier offset frequency and is more than 30 dB above the 300-kHz offset frequency. It has been revealed that the frequency noise of a self-injection–locked

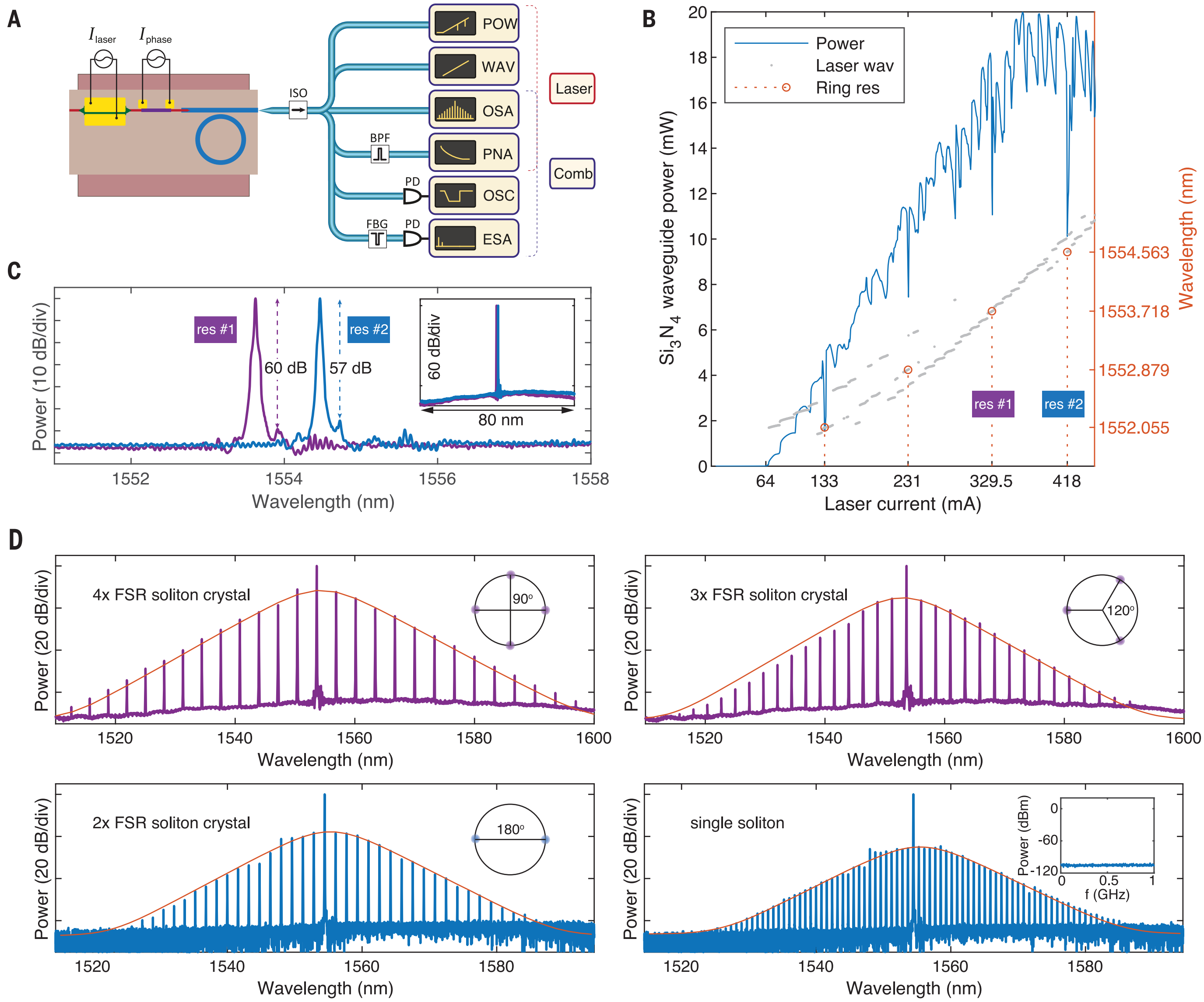

Fig. 3. Device characterization and experimental generation of soliton spectra. (**A**) Experimental setup for laser and soliton characterization. I_{laser} and I_{phase} are the current sources to drive the laser and the phase tuner. POW, power meter; WAV, wavelength meter; OSA, optical spectrum analyzer; PNA, phase noise analyzer; OSC, oscilloscope; ESA, electrical spectrum analyzer; ISO, isolator; BPF, band-pass filter; FBG, fiber Bragg grating; PD, photodetector. (**B**) Light-current sweep measurement with stepped laser current and fixed phase tuner current. Gray color shows the corresponding laser center wavelength as a function of the laser current. Red circles indicate the laser wavelength coinciding with microresonator resonances. Soliton microcombs are generated with laser currents and wavelengths at resonance #1 and resonance #2. (**C**) Single-mode DFB laser spectra at the wavelengths of resonance #1 and resonance #2. (**D**) Optical spectra of soliton states. Inset shows the relative position of multi-solitons circulating inside the microring resonator for four-, three-, and two-FSR soliton crystal states and low-frequency radio-frequency spectrum of the single-soliton state. The applied gain currents to generate these soliton states are shown in (B) for the corresponding resonances, and the phase tuner currents are 11.7 mA for four- and three-FSR states, 15.3 mA for two-FSR and single-soliton states. To switch the soliton state, the gain current is increased together with fine current tuning with 0.1-mA resolution.

laser to a high-Q Si_3N_4 microresonator can be dominantly limited by the thermo-refractive noise of the microresonator (*17*, *31*). Though the free-running linewidth of the DFB laser is broad, owing to the linewidth narrowing provided by self-injection locking, the laser can still directly generate soliton states, surpassing its intrinsic limitation of spectral impurity. Additionally, the coherence of the injection-locked pump line is transferred to other comb lines. For example, the first pair of neighboring comb lines, 100 GHz apart from the pump, have a fundamental linewidth around 200 to 300 Hz, and their frequency noise below 10-MHz offset frequency directly inherits that of the pump line. The self-injection locking scheme thus enables multiwavelength, narrow-linewidth laser sources. Our device represents the realization of a self-injection–locked, narrow-linewidth laser on Si.

Comb generation with self-injection locking relies critically on the phase relation between the forward signal (i.e., the laser emission to the microresonator) and backward signal (i.e., the backscattered light from the microresonator to the laser). In this case, comb generation is only allowed when the optical phase difference is within a certain optimized range. In previous works using hybrid integrated devices (*15*, *16*), controlling the phase difference

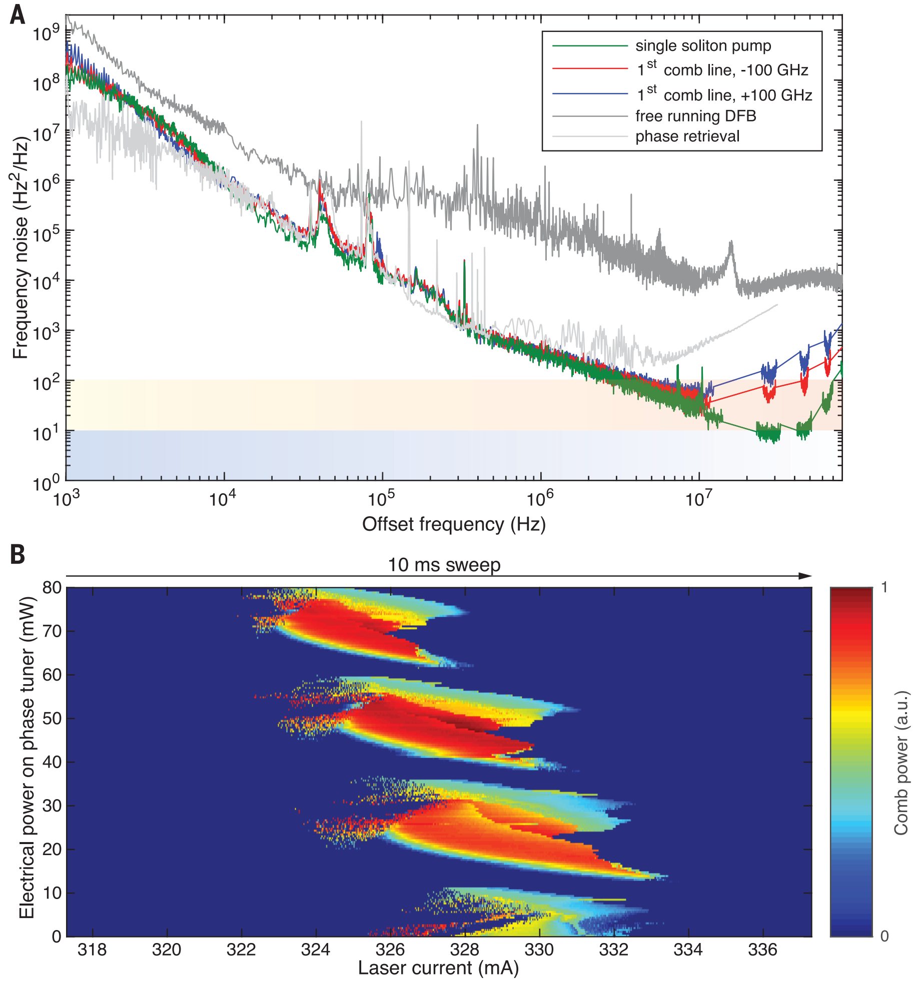

Fig. 4. Laser frequency noise spectra and comb generation with self-injection locking. (**A**) Frequency noise spectra of the self-injection–locked pump line (green), comb lines with ±100-GHz frequency offset to the pump (blue and red) in the single-soliton state, free-running single-mode DFB laser output without self-injection locking (dark gray), and comb line around 1550 nm for the two-FSR soliton crystal state using optical phase retrieval method (*25*). (**B**) Comb power evolution with sweeping laser current (10 ms sweep) under varying electrical power on the phase tuner.

was realized by varying the gap distance between the laser chip and Si_3N_4 chip, which, however, also caused the power coupling efficiency between these two chips to fluctuate. In our monolithic device, this optical phase difference can be directly controlled by varying the phase-tuner current. We experimentally study the comb formation with laser current sweep under different currents on the phase tuner. To exclude the interference from the mode-hop phenomenon when monitoring the power of the new frequency components, we sweep the laser current across the resonance #1 shown in Fig. 3B. Results shown in Fig. 4B reveal that the comb generation is only permitted with certain phase conditions. More study (*25*) indicates that the backscattered signal needs to be in phase with the forward signal. Additionally, the phase-altering effect is periodic and deterministic with the applied electrical power on the phase tuner. Thus, the allowed comb generation regime depends mainly on the pump power and the intensity of the backscattered light (*25*).

In sum, we have presented a heterogeneously integrated laser soliton microcomb on silicon. The device outputs a single soliton with a 100-GHz repetition rate and exhibits self-injection–locked laser performance with frequency noise reduction. More functions can be added into our current technology with other material platforms (*25*). Our process can be upgraded to 200- or 300-mm-diameter substrates by using modified CMOS foundry pilot lines and transfer heterogeneous integration to scalable production of chip-scale frequency combs for field-deployable applications.

REFERENCES AND NOTES

1. S. A. Diddams, K. Vahala, T. Udem, *Science* **369**, eaay3676 (2020).
2. T. Fortier, E. Baumann, *Commun. Phys.* **2**, 153 (2019).
3. T. J. Kippenberg, A. L. Gaeta, M. Lipson, M. L. Gorodetsky, *Science* **361**, eaan8083 (2018).
4. D. J. Moss, R. Morandotti, A. L. Gaeta, M. Lipson, *Nat. Photonics* **7**, 597–607 (2013).
5. A. L. Gaeta, M. Lipson, T. J. Kippenberg, *Nat. Photonics* **13**, 158–169 (2019).
6. Y. Xuan *et al.*, *Optica* **3**, 1171 (2016).
7. M. H. P. Pfeiffer *et al.*, *Optica* **3**, 20 (2016).
8. X. Ji *et al.*, *Optica* **4**, 619 (2017).
9. J. Liu *et al.*, *Nat. Commun.* **12**, 2236 (2021).
10. J. Liu *et al.*, *Nat. Photonics* **14**, 486–491 (2020).
11. L. Maleki *et al.*, *2010 IEEE International Frequency Control Symposium* (2010), pp. 558–563.
12. W. Liang *et al.*, *Nat. Commun.* **6**, 7957 (2015).
13. W. Liang *et al.*, *Nat. Commun.* **6**, 7371 (2015).
14. N. M. Kondratiev *et al.*, *Opt. Express* **25**, 28167 (2017).
15. B. Shen *et al.*, *Nature* **582**, 365–369 (2020).
16. A. S. Voloshin *et al.*, *Nat. Commun.* **12**, 235 (2021).
17. W. Jin *et al.*, *Nat. Photonics* **15**, 346–353 (2021).
18. B. Stern, X. Ji, Y. Okawachi, A. L. Gaeta, M. Lipson, *Nature* **562**, 401–405 (2018).
19. T. Komljenovic *et al.*, *J. Lightwave Technol.* **34**, 20–35 (2016).
20. J. Zhang *et al.*, *APL Photonics* **4**, 110803 (2019).
21. D. Liang, J. E. Bowers, *Light Adv. Manuf.* **2**, 5 (2021).
22. J. Sun, E. Timurdogan, A. Yaacobi, E. S. Hosseini, M. R. Watts, *Nature* **493**, 195–199 (2013).
23. R. Jones *et al.*, *IEEE Nanotechnol. Mag.* **13**, 17–26 (2019).
24. C. Xiang *et al.*, *Optica* **7**, 20 (2020).
25. See supplementary materials.
26. D. Liang, J. E. Bowers, *J. Vac. Sci. Technol. B Microelectron. Nanometer Struct. Process. Meas. Phenom.* **26**, 1560 (2008).
27. W. Jin *et al.*, *Opt. Lett.* **45**, 3340–3343 (2020).
28. M. L. Davenport *et al.*, *IEEE J. Sel. Top. Quantum Electron.* **22**, 78–88 (2016).
29. L. A. Coldren, S. W. Corzine, M. Mashanovitch, *Diode Lasers and Photonic Integrated Circuits* (Wiley, 2012).
30. M. Karpov *et al.*, *Nat. Phys.* **15**, 1071–1077 (2019).
31. G. Huang *et al.*, *Phys. Rev. A* **99**, 061801 (2019).
32. C. Xiang, J. Liu, Open data for "Laser soliton microcombs heterogeneously integrated on silicon,"version 1, Zenodo (2021); https://doi.org/10.5281/zenodo.4745864.

ACKNOWLEDGMENTS

We thank M. Dumont and J. He for help in device characterization and W. Jin for help in mode simulations. **Funding:** This publication was supported by the Defense Advanced Research Projects Agency (DARPA) under DODOS (HR0011-15-C-055) programs of the Microsystems Technology Office (MTO), by the Air Force Office of Scientific Research under Award no. FA8655-20-1-7009, and by the Swiss National Science Foundation under grant agreement no. 176563 (BRIDGE). J.R. acknowledges support from the EUs H2020 research and innovation program under the Marie Sklodowska-Curie IF grant agreement no. 846737 (CoSiLiS). **Author contributions:** C.X., J.L., and L.C. designed the wafer layout and process flow. J.L. and R.N.W. fabricated the Si_3N_4 substrate. C.X. and J.P. fabricated the heterogeneous InP/Si lasers and Si circuits with assistance from W.X. and Z.Z. C.X., J.G., and J.L. tested the final chips. C.X. and J.G. performed the laser soliton experiments with assistance from J.L. and J.R. W.W. performed the numerical simulations of self-injection locking. J.S. took the FIB-SEM image. C.X., J.L., and W.W. wrote the manuscript, with input from others. T.J.K. and J.E.B supervised the project. **Competing interests:** J.E.B.is a cofounder and shareholder of Nexus Photonics and Quintessent, startups in silicon photonics. T.J.K. is a cofounder and shareholder of LiGenTec SA, a start-up company that is engaged in making Si_3N_4 nonlinear photonic chips available through foundry service. **Data and materials availability:** The datasets are available through Zenodo (*32*).

SUPPLEMENTARY MATERIALS

science.sciencemag.org/content/373/3550/99/suppl/DC1
Materials and Methods
Supplementary Text
Figs. S1 to S7
Tables S1 and S2
References (*33*–*51*)

22 February 2021; accepted 20 May 2021
10.1126/science.abh2076

Science

Laser soliton microcombs heterogeneously integrated on silicon

Chao Xiang, Junqiu Liu, Joel Guo, Lin Chang, Rui Ning Wang, Wenle Weng, Jonathan Peters, Weiqiang Xie, Zeyu Zhang, Johann Riemensberger, Jennifer Selvidge, Tobias J. Kippenberg and John E. Bowers

Science **373** (6550), 99-103.
DOI: 10.1126/science.abh2076

Chip-based frequency combs

The realization of optical frequency combs, light sources with precisely spaced frequencies across a broad spectrum of wavelengths, in dielectric microresonators has affected a range of applications from imaging and ranging to precision time keeping and metrology. Xiang *et al.* demonstrate that the entire system, the laser-pumping system and the comb-generating microresonators, can be combined into an integrated silicon-based platform. Compatibility with foundry fabrication methods will enable this innovation to have a major impact on coherent communications, optical interconnects, and low-noise microwave generation.

Science, abh2076, this issue p. 99